Analytic Solutions of Flowfields Inside a Rolling Deformed Torus

Youn J. Kim*

(Received March 4, 1996)

The flowfields inside a deformed rolling torus are analyzed in the limit where the cross-sectional diameter is small in comparison to the torus diameter. The geometric domain consists of a torus whose cross-section is circular except in the footprint region where the cross-section is flattened. Analytic formulas for the flow velocities and pressures are derived and followed by a coordinate transformation. Results for the pressure fields are presented with the Poiseuille flow limit.

Key Words: Poiseuille Flow, Deformed Torus, Secondary Flow.

Nomenclature

A	:	Major axis of elliptic cross section.
B	:	Minor axis of elliptic cross section.
a	:	Undeformed cross-sectional radius of torus.
c	:	Wall velocity in the z-direction.
L	:	Half length of the deformed region
ℓ	:	Half the total length of the torus
$\dot{m}$	:	Mass flowrate
P	:	Dimensinless pressure
p	:	Pressure
R	:	Local radius of the torus cross section
r,θ,z	:	Cylindrical coordinates
Re	:	Reynolds number($=\frac{ca}{\nu}$)
s	:	Arc length in the θ-direction
t	:	Time
u,v,w	:	Velocity components in radial(r), angular(θ), and axial(ϕ) directions
$v_x,v_y,w(U,V,W')$	:	Velocity components(dimensionless) in the cartesian coordinates
w'	:	The increment in the ϕ-component of velocity
$x,y,z(\xi,\eta,\zeta)$	:	Cartesian(dimensionless) coordinates
δ_{max}	:	Maximum radial displacement of the deformed torus
$\tilde{\xi},\tilde{\eta}$	:	Transformed coordinates of the cross-sectional Plane of ellipse
μ	:	Fluid viscosity
ν	:	Fluid kinematic viscosity
ρ	:	Fluid density
σ	:	Cylindrical radius
Ω	:	Angular velocity of rotating torus

* School of Mechanical Engineering Sung Kyun Kwan University, Suwon 440-746, Korea

1. Introduction

Recently, the development of auto industry with high performance characteristics has shown increasing concern about reducing tire rolling power losses to improve vehicle fuel economy, because six percent of the total energy utilized by an automibile is assumed by rolling resistance of the tires. Thus, a need exists for the development of methods for predicting the internal flowfields.

The present paper seeks to extend the analysis of Rae (1983) to nonzero values of the Reynolds number and ratio of cross sectional diameter to

wheel diameter, and to more realistic models of the tire cross-sectional shape. The full equations of motion (for steady, three-dimensional viscous flow in a deformed torus with a moving wall) are presented in Sec. 2, followed by a discussion of the geometric parameters that characterize the problem. Some of these parameters are similar to those appearing in the classical problem of fully developed flow in a tightly coiled helix (Dean, 1927 and 1928), and its extensions to entrance effects (Yao and Berger, 1975, Talbot and Wong, 1982, Stewartson *et al.*, 1980), and unsteady-flow effects (Chandran *et al.*, 1979, Mullin and Greated, 1980, Lin and Tarbell, 1980). There is a essential difference in the present problem, however, since neither the pressure distribution nor the mass flow is known in advance, and these variables must be found as part of the solution. In addition, the deformation of the tire introduces significant geometrical complication and the moving-wall boundary condition necessitates matching of the flow velocity at the wall to the three components of velocity of the surface itself.

For small values of the radius ratio, the tire geometry approaches that of a pipe whose axis is straight, but whose cross-section is deformed. In this limit, analytic solutions can be found in two cases: the first applies at vanishing Reynolds number, where the appropriate equations are those of Stokes flow, and reduce to Poiseuille flow when the deformation is small enough that the longitudinal components of the shear stress are negligible in comparison to the transverse ones. The solution in this limit is presented in Sec. 3 for a deformation that changes from a circular cross-section to that of an ellipse of equal perimeter.

2. Basic Equations

The coordinates used to describe the region inside the deformed rolling torus are shown in Fig. 1. Here R is the fixed radial location of some convenient point in the toroidal cross section, such as its centroid in the undeformed state. The angle ϕ is measured in the rolling direction, while

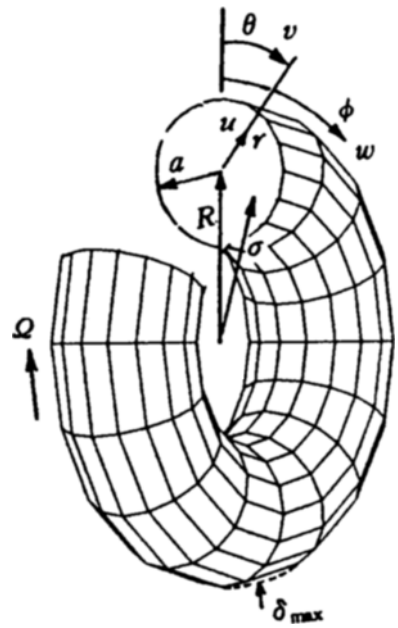

Fig. 1 Toroidal coordinates system.

r and θ are polar coordinates in the cross section. The cylindrical radius is denoted by σ, while u,v and w denote the velocity components in the r,θ and ϕ directions respectively.

For some purpose it is useful to separate the solid-body rotation parts of the pressure and the ϕ-component of velocity, as follows:

$$p=\frac{\rho}{2}(\Omega\sigma)^2+p';\ w=\Omega\sigma+w' \tag{1}$$

where Ω denotes the angular velocity of rotating torus.

The Navier-Stokes equations in these variables are listed in Appendix. This set of equations forms the starting point for the analytic studies of the present paper. Three parameters appear from a dimensional analysis of the problem: a/R, $\Omega Ra/\nu$ and $\delta_{\max}/L$. Here a is a measure of the mean cross-sectional radius of the undeformed torus, $\delta_{\max}$ is the maximum radial displacement of the deformed torus, and L is the half length of the deformed region.

In addition, the entire shape of the deformed torus must be considered as a parameter of the

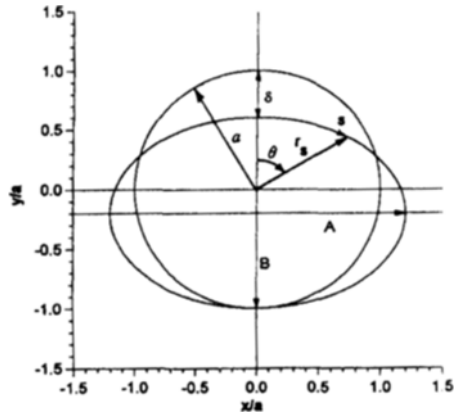

Fig. 2 Deformation of a circle into an ellipse of equal perimeter.

problem: it enters through the torus geometry contained in the function $r_s(\phi,\theta)$. Figure 2 shows the notation; note that the point at $y=-a$ remaining at a constant distance from the axis of rotation. Because the pressures generated by the torus motion are small compared to the inflation pressure, the torus geometry can be regarded as given; there is no interaction between the inner air motion and the torus shape.

The boundary condition to be satisfied is that the fluid velocity of the gas adjacent to the surface be equal to the velocity of the surface. The mechanics of deformation of a torus can be very complicated (Koutny, 1976), but in general it is found that stretching in the θ-direction is small comparison to the compression and extensions that may take place in the ϕ-direction (Hill and Baumgarten, 1984). As a simple model of this behavior, the present study assumes that the perimeter of the toroidal cross section remains constant, while the circumference in the ϕ-direction is compressed by the indentation in the footprint region.

As a consequence of this assumption, the boundary values of the velocity components are

$$w=\Omega\sigma \;;\; w'=0 \tag{2}$$

$$u=\frac{\partial r_s}{\partial t}\Big)_s=\Omega\frac{\partial r_s}{\partial\phi}\Big)_s;v=r_s\frac{\partial\theta}{\partial t}\Big)_s=\Omega r_s\frac{\partial\theta}{\partial\phi}\Big)_s \tag{3a,b}$$

where s is the arclength in the θ-direction. A more convenient form of these expressions can be found by using

$$\frac{\partial r_s}{\partial\phi}\Big)_s=\frac{\partial r_s}{\partial\phi}\Big)_\theta+\frac{\partial r_s}{\partial\theta}\Big)_\phi\frac{\partial\theta}{\partial\phi}\Big)_s \tag{4}$$

and

$$\frac{\partial\theta}{\partial\phi}\Big)_s=-\frac{\partial s/\partial\phi)_\theta}{\partial s/\partial\theta)_\phi} \tag{5}$$

These give

$$u=\Omega\frac{\partial r_s}{\partial\phi}\Big)_\theta+\frac{v}{r_s}\frac{\partial r_s}{\partial\theta}\Big)_\phi;v=-\Omega\, r_s\frac{\partial s/\partial\phi)_\theta}{\partial s/\partial\theta)_\phi} \tag{6a,b}$$

If the arc length and surface-radius variations are given explicitly, these relations can be used directly.

3. Poiseuille-Flow Solutions

The appropriate equations in the thin-tire limit are found by letting the cross-sectional radius r be small in comparison to the wheel radius R. Then $\sigma\simeq R$, and the equations of motion reduce to those in cylindrical coordinates r,θ and z, where $z=R(\phi-\pi)$ is the distance along the cylindrical axis, measured from the center of the footprint region. Because the flows to be considered will not in general be axisymmetric, it is useful to write these equations in cartesian coordinates:

$$\frac{\partial v_x}{\partial x}+\frac{\partial v_y}{\partial y}+\frac{\partial w}{\partial z}=0 \tag{7}$$

$$v_x\frac{\partial v_x}{\partial x}+v_y\frac{\partial v_x}{\partial y}+w\frac{\partial v_x}{\partial z}=-\frac{1}{\rho}\frac{\partial p'}{\partial x}+\nu\nabla^2 v_x \tag{8a}$$

$$v_x\frac{\partial v}{\partial x}+v_y\frac{\partial v_y}{\partial y}+w\frac{\partial v_y}{\partial z}=-\frac{1}{\rho}\frac{\partial p'}{\partial y}+\nu\nabla^2 v_y \tag{8b}$$

$$v_x\frac{\partial w}{\partial x}+v_y\frac{\partial w}{\partial y}+w\frac{\partial w}{\partial z}=-\frac{1}{\rho}\frac{\partial p'}{\partial z}+\nu\nabla^2 w \tag{8c}$$

where v_x and v_y denote the velocity components in the x and y-directions respectively. Here z lies along the axis of the channel, while x and y lie in the cross-sectional plane.

Consider now a pipe whose undeformed cross-sectional scale is a, and has a deformed region of length $2L$ and maximum deflection δ_{max}(see Fig. 1). The velocity of the wall in the z-direction

is called c. Define dimensionless variables by

$$\xi = x/a,\ \eta = y/a,\ \zeta = z/L,\ p = \frac{\mu c}{a}\frac{\delta_{\max}}{a}P$$

$$v_x = c\frac{\delta_{\max}}{L}U,\ v_y = c\frac{\delta_{\max}}{L}V$$

$$w = c\left(1 + \frac{\delta_{\max}}{L}W'\right)$$

In terms of these variables the Navier-Stokes equations become

$$\frac{\partial U}{\partial \xi} + \frac{\partial V}{\partial \eta} + \frac{a}{L}\frac{\partial W'}{\partial \zeta} = 0 \tag{9}$$

$$Re\frac{\delta_{\max}}{L}\frac{a}{L}\left(U\frac{\partial U}{\partial \xi} + V\frac{\partial U}{\partial \eta}\right) + Re\left(\frac{a}{L}\right)^2\left(1 + \frac{\delta_{\max}}{L}W'\right)\frac{\partial U}{\partial \zeta} = -\frac{\partial P}{\partial \xi} + \frac{a}{L}\bar{\nabla}^2 U \tag{10a}$$

$$Re\frac{\delta_{\max}}{L}\frac{a}{L}\left(U\frac{\partial V}{\partial \xi} + V\frac{\partial V}{\partial \eta}\right) + Re\left(\frac{a}{L}\right)^2\left(1 + \frac{\delta_{\max}}{L}W'\right)\frac{\partial V}{\partial \zeta} = -\frac{\partial P}{\partial \eta} + \frac{a}{L}\bar{\nabla}^2 V \tag{10b}$$

$$Re\frac{\delta_{\max}}{L}\left(U\frac{\partial W'}{\partial \xi} + V\frac{\partial W'}{\partial \eta}\right) + Re\frac{a}{L}\left(1 + \frac{\delta_{\max}}{L}W'\right)\frac{\partial W'}{\partial \zeta} = -\frac{\partial P}{\partial \zeta} + \bar{\nabla}^2 W' \tag{10c}$$

where

$$\bar{\nabla}^2 = \frac{\partial^2}{\partial \xi^2} + \frac{\partial^2}{\partial \eta^2} + \left(\frac{a}{L}\right)^2\frac{\partial^2}{\partial \zeta^2},\ Re = \frac{ca}{\nu}$$

The Poiseuille-flow limit is now found by taking $Re \to 0$, $a/L \to 0$; the dependent variables are expanded as

$$P = P_0 + \frac{a}{L}P_1 + \mathcal{O}\left(\frac{a}{L}\right)^2 \tag{11a}$$

$$W' = W'_0 + \frac{a}{L}W'_1 + \mathcal{O}\left(\frac{a}{L}\right)^2 \tag{11b}$$

$$U = \frac{a}{L}U_1 + \mathcal{O}\left(\frac{a}{L}\right)^2 \tag{11c}$$

$$V = \frac{a}{L}V_1 + \mathcal{O}\left(\frac{a}{L}\right)^2 \tag{11d}$$

The equations to be solved for the zeroth and first orders are

$$\frac{\partial P_0}{\partial \zeta} = \left(\frac{\partial^2}{\partial \xi^2} + \frac{\partial^2}{\partial \eta^2}\right)W'_0 \tag{12}$$

$$\frac{\partial U_1}{\partial \xi} + \frac{\partial V_1}{\partial \eta} = -\frac{\partial W'_0}{\partial \zeta} \tag{13}$$

$$\frac{\partial P_1}{\partial \xi} = \frac{\partial P_1}{\partial \eta} = 0$$

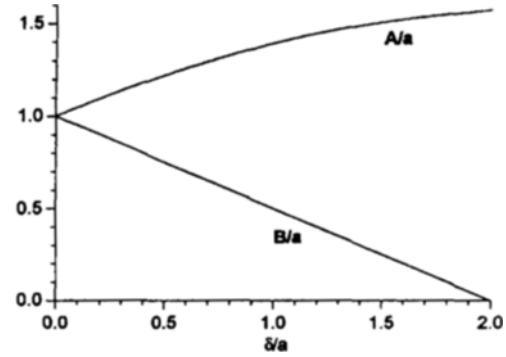

Fig. 3 Relations of major and minor axis.

$$Re\frac{\partial W'_0}{\partial \zeta} = -\frac{\partial P_1}{\partial \zeta} + \left(\frac{\partial^2}{\partial \xi^2} + \frac{\partial^2}{\partial \eta^2}\right)W'_1 \tag{14}$$

The leading term is the Poiseuille-flow approximation, in which the axial pressure gradient is balanced by the transverse shear gradient. The solution for the case of axisymmetric flow (purely radial deformation) is given in Rae (1983). That geometry is not very realistic, since the perimeter of the deformed cross-section is not constant. In what flows, the Poiseuille-flow solution is given for a geometry that changes from a circle to an ellipse of equal perimeter. As shown in Fig. 2, the specific shape used for the case below is given by

$$\frac{\delta}{a} = \frac{\delta_{\max}}{2a}[1 + \cos\{6(\phi - \pi)\}]$$

$$\frac{5\pi}{6} \le \phi \le \frac{7\pi}{6};$$

$$\delta = 0 \text{ else where} \tag{15}$$

with $\delta_{\max}/a = 0.4$. This is the same geometry as used in the calculations of Taulbee *et al.* (1984).

The semi-minor axis of the ellipse is given by

$$\frac{B}{a} = 1 - \frac{1}{2}\frac{\delta}{a} \tag{16}$$

and the semi-major axis follows from the requirement of constant perimeter, which reduce to

$$\frac{A}{a} = \frac{\pi/2}{E(k, \pi/2)},\ k \equiv \left(1 - \frac{B^2}{A^2}\right)^{1/2} \tag{17}$$

where E is the elliptic integral of the second kind (Abramowitz and Stegun, 1970):

$$E(k, \varphi) = \int_0^{\varphi}\sqrt{1 - k^2\sin^2\beta}\, d\beta \tag{18}$$

The variations of A and B with δ are shown in Fig. 3.

3.1 Zeroth-order solution

The solution of Eq. (12) is found by using coordinates in the cross-sectional plane which have their origin at the center of ellipse:

$$\xi = \frac{\xi}{\frac{A}{a}(\zeta)}; \quad \hat{\eta} \frac{\left[\eta - \frac{1}{2}\frac{\delta}{a}(\zeta)\right]}{\frac{B}{a}(\zeta)} \tag{19a,b}$$

The torus surface is then given by $\xi^2 + \hat{\eta}^2 = 1$, and the equation to be solved is

$$\frac{\partial P_o}{\partial \zeta} = \left[\left(\frac{a}{A}\right)^2 \frac{\partial^2}{\partial \xi^2} + \left(\frac{a}{B}\right)^2 \frac{\partial^2}{\partial \hat{\eta}^2}\right] W_o' \tag{20}$$

The solution of this equation is the same as that of Wild *et al.* (1977):

$$W_o'(\hat{\eta}, \xi, \zeta) = -\frac{dP_o}{d\zeta} \frac{\left(\frac{A}{a}\right)^2\left(\frac{B}{a}\right)^2}{2\left[\left(\frac{A}{a}\right)^2 + \left(\frac{B}{a}\right)^2\right]} \times (1 - \xi^2 - \hat{\eta}^2) \tag{21}$$

In Wild *et al.*(1977) the pressure was pre-assigned, and this solution was then used to find the resulting mass flow. In the present case, the pressure will vary with ζ in such a way as to keep the mass flow constant at each ϕ ; this is possible only for one value of the total mass flow. Its determination is as follows. The incremental mass flow due to W_o' is

$$\int_A W_o' dA = -\frac{\pi}{4}\frac{dP_o}{d\zeta} \frac{\left(\frac{A}{a}\right)^2\left(\frac{B}{a}\right)^2}{\left[\left(\frac{A}{a}\right)^2 + \left(\frac{B}{a}\right)^2\right]} \tag{22}$$

or, in dimensional form

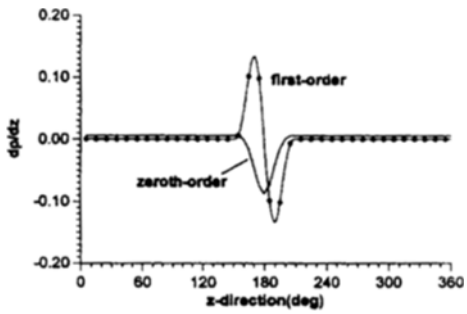

Fig. 4 Pressure-gradient distribution.

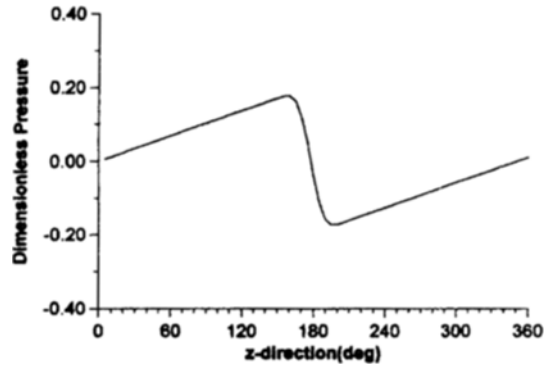

Fig. 5 Poiseuille flow solution for the pressure(zerothorder).

$$\int_A w_o' dx dy = -\frac{\pi}{4\mu} ABa^2 \frac{dp_o}{dz} \frac{\left(\frac{A}{a}\right)^2\left(\frac{B}{a}\right)^2}{\left[\left(\frac{A}{a}\right)^2 + \left(\frac{B}{a}\right)^2\right]} \tag{23}$$

The total mass flow is this amount plus the amount transported by the solid-body rotation:

$$\frac{\dot{m}}{\rho} = \pi ABc - \frac{dp_o}{dz}\frac{\pi a^4}{4\mu} \frac{\left(\frac{A}{a}\right)^3\left(\frac{B}{a}\right)^3}{\left[\left(\frac{A}{a}\right)^2 + \left(\frac{B}{a}\right)^2\right]} \tag{24}$$

Neither of the terms on the right-hand side of this equation is constant; only their sum is required to equal the total flow rate.

This expression can be solved for the pressure gradient:

$$-\frac{dp_o}{dz} = \frac{4\nu}{\pi a^4}(\dot{m} - \pi\rho ABc) \frac{\left[\left(\frac{A}{a}\right)^2 + \left(\frac{B}{a}\right)^2\right]}{\left(\frac{A}{a}\right)^3\left(\frac{B}{a}\right)^3} \tag{25}$$

The periodicity condition on the pressure

$$\int_{-\ell}^{\ell} \frac{dp}{dz} dz = 0 \tag{26}$$

then gives the unique value of the mass flow:

$$\frac{\dot{m}}{\pi\rho c a^2} = \frac{\int_{-\ell}^{\ell} \frac{\left[\left(\frac{A}{a}\right)^2 + \left(\frac{B}{a}\right)^2\right]}{\left(\frac{A}{a}\right)^2\left(\frac{B}{a}\right)^2} dz}{\int_{-\ell}^{\ell} \frac{\left[\left(\frac{A}{a}\right)^2 + \left(\frac{B}{a}\right)^2\right]}{\left(\frac{A}{a}\right)^3\left(\frac{B}{a}\right)^3} dz} \tag{27}$$

Here ℓ is half the total length of the pipe (equal

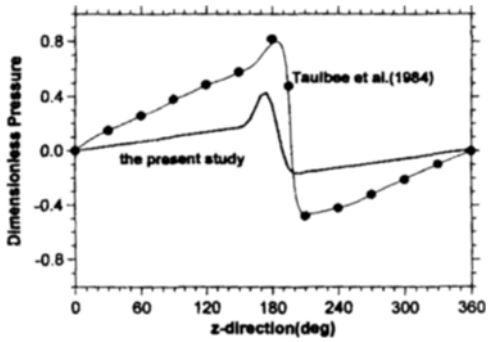

Fig. 6 Comparison of the axial pressure distributions between the result of Taulbee et al. and the present analysis for $Re=10$.

to half the circumference of the thin tire being studied). For the case of a circular cross section($A=B$), these formulas reduce to those of Rae (1983).

Figures 4 and 5 show numerical results for the specific deformation described above, applied to a radius ratio of 1/3 to facilitate comparison with the numerical results of Taulbee *et al.* (1984). In Fig. 6, the comparison of the only distributions of the average axial pressure between the numerical result of Taulbee *et al.* and the present analysis has shown for $Re=10$. Both axial pressure profiles show a similar trend. Such a large curvature parameter, however, clearly violates the thin-tire approximation, and this accounts for some of the difference between the analytic and numerical results.

3.2 First-order solution

The solution for the first-order (in a/L) pressure and axial velocity component can be found as follows: the left-hand side of the last of Eq. (14) is (with $\zeta=\zeta$):

$$\begin{aligned}\frac{\partial W'_o}{\partial\zeta}\Big)_{\xi,\eta}&=\frac{\partial W'_o}{\partial\zeta}\Big)_{\hat\xi,\hat\zeta}+\frac{\partial\hat\eta}{\partial\zeta}\Big)_{\xi,\eta}\frac{\partial W'_o}{\partial\hat\eta}\Big)_{\hat\xi,\hat\zeta}\\&\quad+\frac{\partial\hat\xi}{\partial\zeta}\Big)_{\xi,\eta}\frac{\partial W'_o}{\partial\hat\xi}\Big)_{\hat\xi,\hat\zeta}\\&=-\frac{d^2P_o}{d\zeta^2}G(\zeta)(1-\hat\xi^2-\hat\eta^2)\\&\quad-\frac{dP_o}{d\zeta}\frac{dG}{d\zeta}(1-\hat\xi^2-\hat\eta^2)+2\hat\eta\frac{\partial\hat\eta}{\partial\zeta}\Big)_{\xi,\eta}\\&\quad\frac{dP_o}{d\zeta}G(\zeta)+2\hat\xi\frac{\partial\hat\xi}{\partial\zeta}\Big)_{\xi,\eta}\frac{dP_o}{d\zeta}G(\zeta)\\&=F_1(\zeta)(1-\hat\xi^2-\hat\eta^2)\\&\quad+F_2(\zeta)\hat\eta[1-\hat\eta]+F_3(\zeta)\hat\xi^2\end{aligned}\tag{28}$$

where

$$G(\zeta)=\frac{\bar A^2\bar B^2}{2(\bar A^2+\bar B^2)};\ \bar A\equiv\frac{A}{a},\ \bar B\equiv\frac{B}{a}\tag{29}$$

and where

$$\begin{aligned}F_1&=-GP''_o-G'P'_o=-(GP'_o)'\\F_2&=2P'_oG\frac{\bar B'}{\bar B}\\F_3&=-2P'_oG\frac{\bar A'}{\bar A}\end{aligned}\tag{30a,b,c}$$

A solution of Eq. (14) satisfying the boundary conditions at the surface is

$$\begin{aligned}W'_1=(1-\hat\eta^2-\hat\xi^2)\Big(&c_o(\zeta)+c_1(\zeta)\hat\eta\\&+c_2(\zeta)\hat\eta^2+d_2(\zeta)\hat\xi^2\Big)\end{aligned}\tag{31}$$

$$c_1=\frac{-ReF_2\bar A^2\bar B^2}{2(\bar B^2+3\bar A^2)}$$

$$c_2=\frac{2\bar A^2\bar B^4Re(F_1-F_3)-(12\bar B^2+2\bar A^2)\bar A^2\bar B^2Re(F_1+F_2)}{4\bar A^2\bar B^2-(12\bar B^2+2\bar A^2)(12\bar A^2+2\bar B^2)}$$

$$d_2=\frac{\bar A^2\bar B^2Re(F_1+F_2)-c_2(2\bar B^2+12\bar A^2)}{2\bar B^2}$$

$$c_o=\frac{2\bar B^2d_2+2\bar A^2c_2+\bar A^2\bar B^2(-\frac{dP_1}{d\zeta}-ReF_1)}{2(\bar A^2+\bar B^2)}$$

Determination of the coefficient c_o cannot be done until the pressure gradient $dP_1/d\zeta$ is found; this quantity, in turn, is set by the condition that the increment in mass flow corresponding to the first-order solution be constant, and of such a magnitude as to make the first-order pressure

periodic. The total mass flow is

$$m=\pi a^2\bar{A}\bar{B}\rho c+\frac{\delta_{\max}}{L}a^2\bar{A}\bar{B}\rho c\left(-\frac{\pi}{4}P_o'G+\frac{a}{L}\int W_1 d\bar{\eta}d\bar{\xi}\right) \tag{32}$$

The integral can be evaluated as

$$\int W_1 d\bar{\eta}d\bar{\xi}=\frac{\pi}{2}c_o+\frac{\pi}{8}(c_2+d_2) \tag{33}$$

Thus the first-order increment in mass flow is

$$\begin{aligned}\triangle\dot{m}&=\frac{a\delta_{\max}}{L^2}\pi a^2\rho c\bar{A}\bar{B}\left[\frac{c_o}{2}+\frac{1}{8}(c_2+d_2)\right]\\&\equiv\frac{a\delta_{\max}}{L^2}\pi a^2\rho c\triangle\dot{M}\end{aligned} \tag{34}$$

Solving this for the pressure gradient one finds

$$\begin{aligned}-\frac{dP_1}{d\zeta}=ReF_1&+\frac{4(\bar{A}^2+\bar{B}^2)}{(\bar{A}\bar{B})^3}\triangle\dot{M}\\&-\frac{(c_2+d_2)(\bar{A}^2+\bar{B}^2)}{2(\bar{A}\bar{B})^2}\\&-\frac{2\bar{B}^2d_2+2\bar{A}^2c_2}{(\bar{A}\bar{B})^2}\end{aligned} \tag{35}$$

Then the periodicity requirement:

$$\int_{-\ell/L}^{\ell/L}\frac{dP_1}{d\zeta}d\zeta=0 \tag{36}$$

will be satisfied if $\triangle\dot{m}$ has the value:

$$\triangle\dot{M}=\frac{K}{4\int_{-\ell/L}^{\ell/L}\dfrac{\bar{A}^2+\bar{B}^2}{(\bar{A}\bar{B})^3}d\zeta} \tag{37}$$

where

$$\begin{aligned}K\equiv&-Re\int_{-\ell/L}^{\ell/L}F_1d\zeta\\&+\int_{-\ell L}^{\ell/L}\frac{(c_2+d_2)(\bar{A}^2+\bar{B}^2)}{2(\bar{A}\bar{B})^2}d\zeta\\&+2\int_{-\ell/L}^{\ell/L}\frac{\bar{B}^2d_2+\bar{A}^2c_2}{(\bar{A}\bar{B})^2}d\zeta\end{aligned} \tag{38}$$

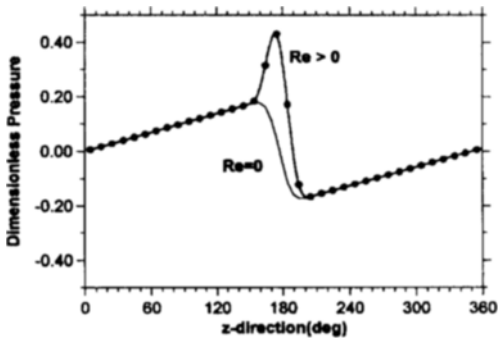

Fig. 7 Pressure distributions.

The geometry used in the present study is symmetric about $\phi=\pi$, and so the quantities F_1, c_2 and d_2 are odd functions of ζ. Thus the value of $\triangle\dot{M}$ in the present case is zero.

Figure 7 shows the zeroth and first-order pressure for the case

$$\frac{a}{R}=\frac{1}{3},\ \frac{\delta_{\max}}{a}=0.4,\ \frac{\ell}{L}=6,\ Re=10$$

and for the deformation given in Eq. (15). As in other studies (Wild *et al.*, 1977), the peak presure gradient is shifted upstream for non-zero Reynolds number.

3.3 Secondary flow

The flow in the planes ζ=constant is given by the velocity components U_1 and V_1, and is referenced to here as the secondary flow. According to the first of Eq. (14), it is not affected by pressure gradients in this plane, but is driven by the wall motions. In order to take these into account, it is necessary to introduce the explicit wall geometry being used. Moreover, because the equations for the surface geometry of the circle-to-ellipse shape are all implicit, it is convenient to consider only the case of small deformations, i.e., $\delta/a\ll1$. For this limit, the major/minor axis ratio is close to 1., and it is possible to derive the following explicit formulas, after some algebra:

$$\frac{B}{a}=1-\frac{1}{2}\frac{\delta}{a}(\text{exact})$$

$$E(k,\theta)=\theta-\frac{k^2}{4}[\theta-\sin\theta\cos\theta]+\bigcirc(k^4) \tag{39a}$$

$$k^2=2\frac{\delta}{a}+\bigcirc\left(\frac{\delta}{a}\right)^2 \tag{39b}$$

$$\frac{B}{A}=1-\frac{\delta}{a}+\bigcirc\left(\frac{\delta}{a}\right)^2 \tag{39c}$$

$$\frac{A}{a}=1+\frac{1}{2}\left(\frac{\delta}{a}\right)+\bigcirc\left(\frac{\delta}{a}\right)^2 \tag{39d}$$

The formulas of cross-sectional shape of the deformed torus are:

$$\frac{x_s}{a}=\sin\frac{s}{a}+\frac{\delta}{2a}\sin^3\frac{s}{a}+\bigcirc\left(\frac{\delta}{a}\right)^2 \tag{40a}$$

$$\frac{y_s}{a}=\cos\frac{s}{a}-\frac{\delta}{2a}\left[1+\cos^3\frac{s}{a}\right]+O\left(\frac{\delta}{a}\right)^2 \quad (40b)$$

$$\frac{r_s}{a}=1+\frac{\delta}{2a}\left[\sin^2\frac{s}{a}-\cos^2\frac{s}{a}-\cos\frac{s}{a}\right]+O\left(\frac{\delta}{a}\right)^2 \quad (40c)$$

$$\theta=\frac{s}{a}+\frac{\delta}{2a}\sin\frac{s}{a}\left(1+\cos\frac{s}{a}\right)+O\left(\frac{\delta}{a}\right)^2 \quad (40d)$$

Thus the velocities of the surface are:

$$u=\left(\frac{\partial r_s}{\partial t}\right)_s=\Omega\left(\frac{\partial r_s}{\partial\phi}\right)_s-\Omega\frac{d\delta}{d\phi}\left(\frac{\partial(r_s/a)}{\partial(\delta/a)}\right)_s$$
$$=\Omega\frac{d\delta}{d\phi}\left\{\frac{1}{2}\left[\sin^2\frac{s}{a}-\cos^2\frac{s}{a}-\cos\frac{s}{a}\right]+O\left(\frac{\delta}{a}\right)\right\} \quad (41)$$

$$v=r_s\left(\frac{\partial\theta}{\partial t}\right)_s=\Omega r_s\left(\frac{\partial\theta}{\partial\phi}\right)_s=\Omega\frac{r_s}{a}\left(\frac{d\delta}{d\phi}\frac{\partial\theta}{\partial(\delta/a)}\right)_s$$
$$-\Omega\frac{d\delta}{d\phi}\left\{\frac{1}{2}\sin\frac{s}{a}\left(1+\cos\frac{s}{a}\right)+O\left(\frac{\delta}{a}\right)\right\} \quad (42)$$

Similarly, the rectangular components are

$$v_x=\Omega\frac{d\delta}{d\phi}\left\{\frac{1}{2}\sin^3\frac{s}{a}+O\left(\frac{\delta}{a}\right)\right\} \quad (43)$$

$$v_y=\Omega\frac{d\delta}{d\phi}\left\{-\frac{1}{2}\left[1+\cos^3\frac{s}{a}\right]+O\left(\frac{\delta}{a}\right)\right\} \quad (44)$$

The exact paths traced by points at given values of s/a are shown in Fig. 2 ; the initial shapes of these trajectories correspond to these approximate formulas for the velocity field. The fact that the trajectories have very little curvature suggests that the approximate formulas are accurate over a significant range of δ/a.

To the accuracy retained, the secondary velocities at the wall can be written as

$$U_1=g(\zeta)\frac{1}{2}\xi^3+O\left(\frac{\delta}{a}\right) \quad (45)$$

$$V_1=g(\zeta)\left\{-\frac{1}{2}(1+\eta^3)\right\}+O\left(\frac{\delta}{a}\right) \quad (46)$$

where

$$g(\zeta)=\frac{\Omega L}{c}\frac{d(\delta/\delta_{\max})}{d\phi}=\frac{\Omega R}{c}\frac{d(\delta/\delta_{\max})}{d\zeta} \quad (47)$$

and where ξ and η can be replaced by $\bar{\xi}$ and $\bar{\eta}$ with no change in the order of the approximation.

Subject to these boundary conditions, the equations to be solved are

$$\frac{\partial U_1}{\partial\xi}+\frac{\partial V_1}{\partial\eta}=\frac{\partial W_0}{\partial\zeta} \quad (48)$$

and a second equation, found by eliminating the pressure from the two secondary-flow momentum equations (and then applying the $a/R\to 0$ limit):

$$\frac{\partial}{\partial\eta}\left(\frac{\partial^2}{\partial\xi^2}+\frac{\partial^2}{\partial\eta^2}\right)U_1=\frac{\partial}{\partial\xi}\left(\frac{\partial^2}{\partial\xi^2}+\frac{\partial^2}{\partial\eta^2}\right)V_1 \quad (49)$$

An approximate solution of this problem was sought as follows: first, the continuity equation is written in the form:

$$\frac{1}{A}\frac{\partial U_1}{\partial\bar{\xi}}+\frac{1}{B}\frac{\partial V_1}{\partial\bar{\eta}}=-[F_1+F_2\bar{\eta}-(F_1+F_2)\bar{\eta}^2-(F_1-F_3)\bar{\xi}^2] \quad (50)$$

A trial solution of this equation, of the form:

$$U_1=\frac{1}{2}g(\zeta)\bar{\xi}^3+\bar{A}(1-\bar{\eta}^2-\bar{\xi}^2)e_1\bar{\xi} \quad (51)$$

$$V_1=-\frac{1}{2}g(\zeta)(1+\bar{\eta}^3)+\bar{B}(1-\bar{\eta}^2-\bar{\xi}^2)(f_0+f_1\bar{\eta}) \quad (52)$$

satisfies the boundary conditions, and would satisfy the differential equation if values of e_1, f_0 and f_1 could be found such that

$$e_1=\frac{3}{4}\frac{g}{\bar{A}}+\frac{1}{2}F_3$$
$$=\frac{3}{4}\frac{g}{\bar{B}}-\frac{1}{2}F_2-F_1$$

$$f_0=\frac{1}{2}F_2$$

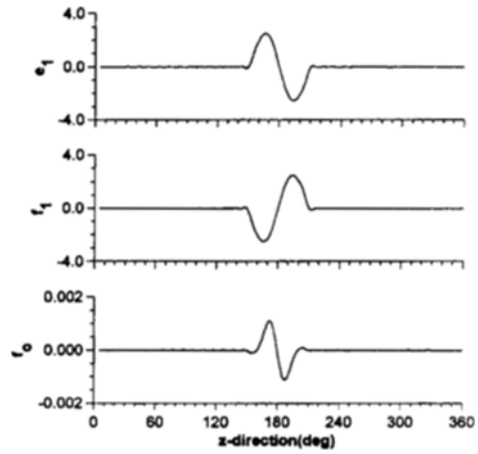

Fig. 8 Variations of parametiers along the z-direction.

$$f_1 = -\frac{3}{4}\frac{g}{A} - F_1 - \frac{1}{2}F_3$$

$$= -\frac{3}{4}\frac{g}{B} - \frac{1}{2}F_2$$

In the above equations, both F_2 and F_3 depend only on δ/a. The variations of e_1, f_o and f_1 along the z-direction are shown in Fig. 8.

4. Conclusions

The full problem of flowfield inside a rolling tire is very complex, and requires solution of the equations of steady motion in a deformed torus, with a moving-wall boundary condition and with a pressure distribution and mass flow that must be found as part of the solution. These degrees of complexity distinguish this problem from other cases of flow in curved passages, such as the Dean problem, where a smaller number of independent parameters is sufficient to define the flow. The present problem is characterized by three parameters: the radius ratio, the Reynolds number, and the tire deflection, as well as the entire surface geometry.

For small values of these parameters, analytic solutions are possible, and one such limiting solution is given in this study. Further studies are required, in order to shed light on the influence of non-zero Reynolds number and curvature. These further studies will also improve understanding of the secondary-flow patterns, radial migration of axial velocity profiles, and other features including temperature distributions that have been observed in numerical solutions of the full equations of motion.

References

Abramowitz, M. and Stegun, I. A., 1970, "Handbook of Mathematical Functions: with Formulas, Graphs, and Mathematical Tables," 9th ed., Dover, New York.

Chandran, K. B., Yearwood, T. L. and Wieting, D. W., 1979, "An Experimental Study of Pulsatile Flow in a Curved Tube," *J. Biomechanics*, Vol. 12, pp. 793~805.

Dean, W. R., 1927, "Note on the Motion of Fluid in a Curved Pipe," *Phil. Mag.* (7) 4, pp. 208~233.

Dean, W. R., 1928, "The Streamline Motion of Fluid in a Curved Pipe," *Phil. Mag.* (7) 5, pp. 673~695.

Hill, D. E. and Baumgarten, J. R., 1984, "Experimental Stress Analysis of a Thin Walled Pressurized Torus Loaded by Contact with a Plane," *AIAA J.*, Vol. 22, pp. 124~127.

Koutny, F., 1976, "A Method for Computing the Radial Deformation Characteristics of Belted Tires," *Tire Science and Technology*, Vol. 4, pp. 190~212.

Lin, J. Y. and Tarbell, J. M., 1980, "An Experimental and Numerical Study of Periodic Flow in a Curved Tube," *J. Fluid Mech.*, Vol. 100, pp. 623~638.

Mullin, T. and Greated, C. A., 1980, "Oscillatory Flow in Curved Pipes. Part I. The Developing-Flow Case," *J. Fluid Mech.*, Vol. 98, pp. 383~395.

Rae, W. J., 1983, "Flow Inside a Pneumatic Tire: A Peristaltic-Pumping Analysis for the Thin-Tire Limit at Very Low Forward Speed," *J. of Applied Mechanics*, Vol. 105, pp. 255~258.

Stewartson, K., Cebeci, T. and Chang, K. C., 1980, "A Boundary-Layer Collision in a Curved Duct," *Q. J. Mech. Appl. Math.*, Vol. 33, pp. 59~75.

Talbot, L. and Wong, S. J., 1982, "A Note on Boundary-Layer Collision in a Curved Pipe," *J. Fluid Mech.*, Vol. 122, pp. 505~510.

Taulbee, D. B., Wey, M. J. and Rae, W. J., 1984, "Calculation of Flow Inside a Loaded Rotating Tire," *the 37th Annual Meeting, American Physical Society, Division of Fluid Dynamics*, Providence, RI.

Wild, R., Pedley, T. J. and Riley, D. S., 1977, "Viscous Flow in Collapsible Tubes of Slowly Varying Elliptical Cross Section," *J. Fluid Mech.*, Vol. 81, pp. 273~294.

Yao, L. S. and Berger, S. A., 1975, "Entry Flow in a Curved Pipe," *J. Fluid Mech.*, Vol. 67, pp. 177~196.

Appendix

Continuity:

$$\frac{\partial u}{\partial r}+\frac{u}{r}+\frac{1}{r}\frac{\partial v}{\partial \theta}+\frac{u\cos\theta-v\sin\theta}{\sigma}+\frac{1}{\sigma}\frac{\partial w'}{\partial \phi}=0$$

r-direction momentum:

$$u\frac{\partial u}{\partial r}+\frac{u}{r}\frac{\partial u}{\partial \theta}-\frac{v^2}{r}+(\Omega+\frac{w'}{\sigma})\frac{\partial u}{\partial \phi}-2\Omega w'\cos\theta-\frac{w'^2\cos\theta}{\sigma}=-\frac{1}{\rho}\frac{\partial p'}{\partial r}-\nu\left\{\frac{1}{\mathrm{r}}\frac{\partial^2 v}{\partial r\partial\theta}+\frac{1}{r^2}\frac{\partial v}{\partial\theta}-\frac{1}{r^2}\frac{\partial^2 u}{\partial\theta^2}-\frac{\sin\theta}{\sigma}\left[\frac{\partial v}{\partial r}+\frac{v}{r}-\frac{1}{r}\frac{\partial u}{\partial\theta}\right]+\frac{1}{\sigma}\frac{\partial^2 w'}{\partial r\partial\phi}-\frac{1}{\sigma^2}\left[\frac{\partial^2 u}{\partial\phi^2}-\cos\theta\frac{\partial w'}{\partial\phi}\right]\right\}$$

θ-direction momentum:

$$u\frac{\partial v}{\partial r}+\frac{v}{r}\frac{\partial v}{\partial\theta}+(\Omega+\frac{w'}{\sigma})\frac{\partial v}{\partial\phi}+\frac{uv}{r}+2\Omega w'\sin\theta+\frac{w'^2\sin\theta}{\sigma}=-\frac{1}{\rho r}\frac{\partial p'}{\partial\theta}+\nu\left\{\frac{\partial^2 v}{\partial r^2}+\frac{1}{r}\frac{\partial v}{\partial r}-\frac{1}{r}\frac{\partial^2 u}{\partial\theta\partial r}-\frac{v}{r^2}+\frac{1}{r^2}\frac{\partial u}{\partial\theta}+\frac{\cos\theta}{\sigma}\left[\frac{\partial v}{\partial r}+\frac{v}{r}-\frac{1}{r}\frac{\partial u}{\partial\theta}\right]-\frac{1}{\sigma r}\frac{\partial^2 w'}{\partial\theta\partial\phi}+\frac{1}{\sigma^2}\left[\frac{\partial^2 v}{\partial\phi^2}+\sin\theta\frac{\partial w'}{\partial\phi}\right]\right\}$$

z-direction momentum:

$$u\frac{\partial w'}{\partial r}+\frac{v}{r}\frac{\partial w'}{\partial\theta}+2\Omega(u\cos\theta-v\sin\theta)+(\Omega+\frac{w'}{\sigma})\frac{\partial w'}{\partial\phi}+\frac{w'}{\sigma}(u\cos\theta-v\sin\theta)=-\frac{1}{\rho\sigma}\frac{\partial p'}{\partial\phi}+\nu\left\{\frac{\partial^2 w'}{\partial r^2}+\frac{1}{r}\frac{\partial w'}{\partial r}+\frac{1}{r^2}\frac{\partial^2 w'}{\partial\theta^2}-\frac{1}{\sigma}\left(\frac{\partial^2 u}{\partial r\partial\phi}-\cos\theta\frac{\partial w'}{\partial r}+\frac{\sin\theta}{r}\frac{\partial w'}{\partial\theta}+\frac{1}{r}\frac{\partial u}{\partial\phi}+\frac{1}{r}\frac{\partial^2 v}{\partial\theta\partial\phi}\right)-\frac{1}{\sigma^2}\left(w'-\cos\theta\frac{\partial u}{\partial\phi}+\sin\theta\frac{\partial v}{\partial\phi}\right)\right\}$$